INTERFACE SCIENCE 6, 287–298 (1998)

Vacancy Generation During Grain Boundary Migration

M. UPMANYU AND D.J. SROLOVITZ
Department of Materials Science and Engineering, University of Michigan, Ann Arbor, MI 48109-2136, USA
Srol@engin.umich.edu

L.S. SHVINDLERMAN
Institute of Solid State Physics, Russian Academy of Sciences, Chernogolovka, Moscow distr. 142432, Russia; and Institut für Metallkunde und Metallphysik, RWTH Aachen, 52 56 Aachen, Germany

G. GOTTSTEIN
Institut für Metallkunde und Metallphysik, RWTH Aachen, 52 56 Aachen, Germany
gg@hp1.imm.rwth-aachen.de

Abstract. We present a molecular dynamics simulation study of vacancy generation and emission from grain boundaries during curvature-driven grain boundary migration. The U-shaped half-loop bicrystal geometry is employed in order to maintain a constant driving force during boundary migration. Nonlinearities in plots of half-loop grain area versus time indicate the onset of non-steady-state behavior and vacancy formation. Such events appear much more frequently at elevated temperature than at low temperature. Detailed observation of the atomic configurations in the vicinity of the grain boundary before and after these events clearly demonstrate that these nonlinearities are associated with the generation and subsequent emission of vacancies. The excess volume associated with the grain boundaries in conjunction with the loss in grain boundary area during curvature-driven migration accounts for the generation of these vacancies. This description is used to predict the rate of vacancy emission, which represents an upper bound on the observed emission rates.

Keywords: curvature-driven grain boundary migration, grain boundary mobility, grain boundary excess volume, vacancy generation, grain boundary pinning, molecular dynamics, Lennard-Jones potential

1. Introduction

Nonconservative motion of an interface occurs when the interface acts as a source or sink for a flux of atoms or point defects. This source/sink behavior requires the creation or destruction of lattice sites at the interface, resulting in the motion of the interface relative to the adjoining crystals. Interface migration kinetics can be divided into diffusion-controlled, interface reaction-controlled and mixed, depending on what controls the rate of absorption of atoms or point defects (which in turn is coupled to the interface motion). Grain boundaries can act as sources or sinks for point defects or short circuit transport paths. Most models for the source/sink behavior of grain boundaries describe the process in terms of the climb of primary or secondary dislocations. If these dislocation have Burgers vectors which are not exactly perpendicular to the grain boundary, then the climb of these dislocations, by necessity, also involves some component of boundary migration [1–3].

Grain boundaries commonly exhibit a different density than the perfect crystals bounding them because the grain boundary and perfect crystal structures are unlike. While there is no restriction that grain boundaries are less dense than the bulk, an excess grain boundary volume has been observed in both experiments and simulations [4–10]. If the total area of the grain boundaries in the material decreases, like in grain growth,

then the excess volume associated with the destruction of the grain boundaries must be accommodated by the bulk. This excess volume may be either in the form of point defects or lattice strains. In curvature-driven boundary migration, the total grain boundary area decreases resulting in a flux of point defects to or from the grain boundary.

A flux of point defects to or from grain boundaries due to grain boundary migration has been postulated, yet never observed or investigated in detail. A simulation study on abnormal grain growth by Srolovitz et al. did hypothesize generation of point defects from grain boundaries [11]. In another simulation study, Wang and Vitek postulated the ejection of vacancies from grain boundaries during grain boundary migration [12]. In this case, the ejection of the vacancy during migration resulted from or causes a local change in the grain boundary structure. Gottstein, Lücke and Estrin [13, 14] as well as Gleiter [15] derived the steady-state vacancy concentration around a moving grain boundary by assuming that the grain boundaries are perfect sources and sinks for vacancies and examined the effects of the resultant vacancies on grain boundary mobility.

In this study, we perform atomistic computer simulations of steady-state, curvature-driven grain boundary migration. The reduction of grain boundary area during boundary migration leads to the generation and subsequent emission of vacancies from the grain boundary. The generation of these point defects is analyzed in terms of the initial grain boundary excess volume present in the system. The relationship between this type of vacancy generation, elastic stresses and other defects are discussed.

2. Simulation Method

The present simulations were performed in two dimensions using the molecular dynamics simulation method and simple, empirical (Lennard-Jones) pair potentials, as described in detail in [16]. These simulations were performed at constant temperature. The crystal structure is a triangular lattice. The basic unit of simulation time for a simple Lennard-Jones potential is $\tau = (mr_0/\varepsilon)^{1/2}$, where m is the atomic mass, r_0 is the nearest neighbor spacing and ε is the depth of the potential well.

In order to measure steady-state grain boundary migration, the simulation geometry must be chosen such

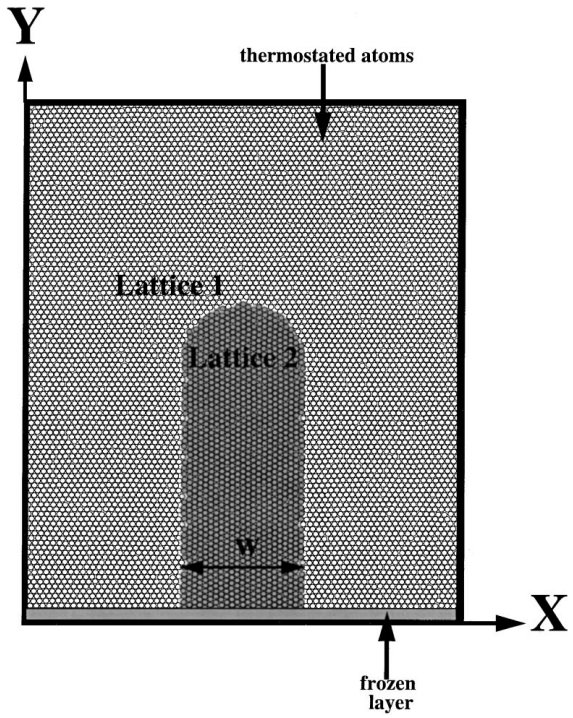

Figure 1. The initial configuration of the simulation cell in the X-Y plane containing the U-shaped half-loop grain boundary (width w). The bottom three layers are frozen at 0 K while the remaining atoms are thermostated at the desired temperature. All of the remaining surfaces are free.

that the driving force does not change during the migration process. In the present simulation, the only driving force is that associated with grain boundary curvature. Shvindlerman and co-workers [17–19] introduced the U-shaped half-loop bicrystal geometry in order to study steady state, curvature-driven boundary migration. This geometry is inherently two-dimensional in that the grain boundary traverses the entire thickness of the thin samples and remains nearly perpendicular to the surface during grain boundary migration. We employ the same U-shaped, half-loop bicrystal geometry in the present two-dimensional simulations and constrain the sample to lie entirely in the X-Y plane (see Fig. 1), as described in detail in [16].

Simulations were performed with bicrystal misorientations corresponding to general ($\Sigma = \infty$ (30°)) and singular (low Σ: $\Sigma = 7$ (38.22°)) boundaries, as described by the coincidence site lattice (CSL) scheme for grain boundary structure. The excess boundary volume was determined for each of these using the Gibbs procedure [20, 21]—i.e., subtract the volume

of the system containing the grain boundary from that of the identical perfect single crystal (containing the same number of atoms) and divide by the total length of grain boundary. The rate of change of the area of the half-loop (Lattice 2 in Fig. 1) $\dot{A}$, is simply the product of the width of the half-loop, w, and the velocity, v, of its tip (in the Y direction); $\dot{A} = vw$ assuming a steady state half-loop shape. If the migration is driven by the grain boundary curvature, we may write $\dot{A}$ as

$$\dot{A} = vw = (M\gamma\kappa)w\left(M\gamma\frac{2}{w}\right)w = 2M\gamma \qquad (1)$$

where γ is the grain boundary (surface) tension, κ is the curvature at the top of the half-loop and M is the grain boundary mobility. Equation (1) implies that for steady-state migration, the rate of change of area of the U-shaped grain is independent of half-loop width and is a measure of the reduced grain boundary mobility, $M\gamma$.

3. Results

The evolution of the area of the half-loop A at low temperature ($T = 0.145\varepsilon/k$, where k is the Boltzmann constant, $w = 21r_0$, $\Sigma = \infty\,(30^\circ)$) is shown in Fig. 2. This plot shows that aside from noise, that A is a linearly decreasing function of time (at late time, the half-loop profile is affected by the presence of the bottom of the simulation cell). The linearity of this plot is consistent with the prediction of Eq. (1), thereby implying that grain boundary velocity is proportional to grain boundary curvature. The slope of this linear plot is proportional to the reduced mobility, $-2M\gamma$. The noise in this plot is associated with thermal fluctuations of the grain boundary.

Figure 3 also shows the evolution of the area of a half-loop, as in Fig. 2, but for the case of a higher symmetry boundary at a higher temperature ($T = 0.175\varepsilon/k$, $w = 21r_0$ and $\Sigma = 7\,(38.22^\circ)$). While Figs. 2 and 3 show the same general form as each other: following an extended initial transient, A decreases

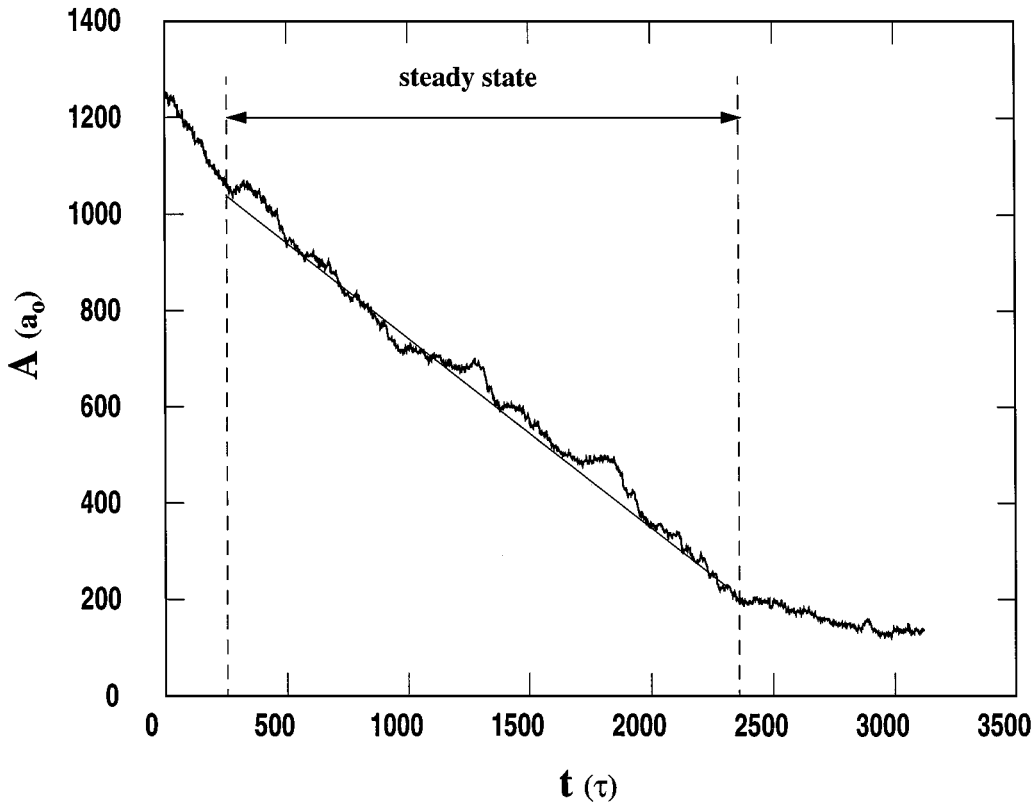

Figure 2. Variation of the area of the half-loop grain A (Lattice 2 in Fig. 1) with time t in a simulation performed at $T = 0.145\varepsilon/k$, $w = 21r_0$ and $\Sigma = \infty\,(30^\circ)$. The solid line represents a best linear fit to the data over the length of the line.

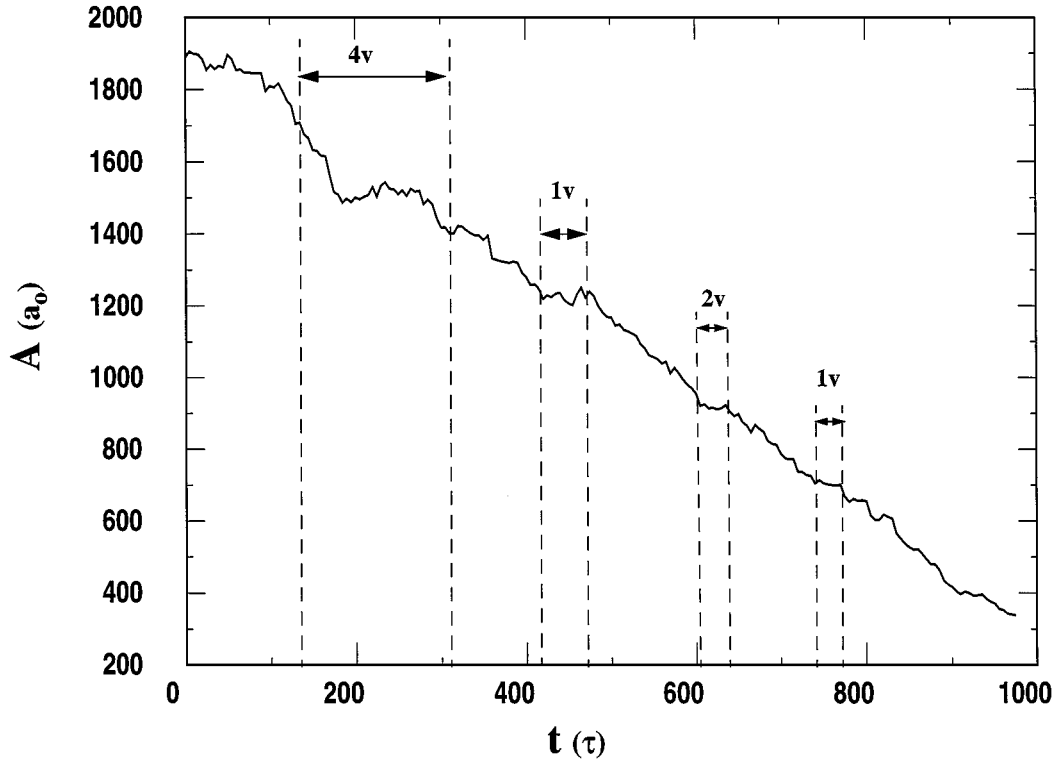

Figure 3. Variation of the area of the half-loop grain with time in a simulation performed at $T = 0.175\varepsilon/k$, $w = 21r_0$ and $\Sigma = 7\,(38.22^\circ)$. The notation nv, where $1 \leq n \leq 4$, indicates the number of vacancies within a nano-void ejected over the time period between the vertical dashed lines and indicated by the double headed arrows.

linearly with time. During this transient, around $t = 200\tau$, the area of the half-loop plateaus, followed by the linear decrease with time. This observation led us to re-examine the A vs. t plot more closely. We observe similar, but smaller, plateaus at later times (e.g., near $t = 450\tau$, $t = 620\tau$). Small plateaus were also observed in low temperature simulations (see Fig. 2). This behavior is difficult to understand on the basis of Eq. (1). It suggests that the shrinking of the half-loop may not be perfectly steady state: either fluctuations are important in how the grain shrinks or there is some key physics missing from our analysis of half-loop shrinking.

In order to determine the origin of these apparent deviations from steady-state, we examine the temporal evolution of the atomic configurations in the vicinity of the half-loop (see Fig. 4) for the case observed in Fig. 3. Following an initial, short time transient wherein the initial, as-constructed boundary equilibrates and establishes the self-similar profile (Fig. 4(a)), boundary migration begins. After the half-loop has retracted a finite distance ($\sim 13r_0$), a small void ($4a_0$, where a_0 is the area associated with a single atom $a_0 = r_0^2\,(3^{3/2})/8$) begins to form near the top of the half-loop (Fig. 4(b)). Once the vacancy forms, it appears to retard further retraction of the half-loop. Following the formation of the nanovoid or vacancy aggregate, the half-loop changes shape (sharpens) with little change in area. This corresponds to the onset of the non-steady-state behavior (i.e., the beginning of the plateau) observed in the A vs. t plot in Fig. 3. At $t \approx 310\tau$, the grain boundary finally pulls away from the vacancy aggregate and returns to its more rounded shape (close to its steady-state form) as it continues to retract (Fig. 4(c)). It is during this period that the A vs. t plot (Fig. 3) starts to become linear.

Examination of the atomic-level pressure (not shown) indicates that a tensile region forms above the ejected vacancy aggregate (Fig. 4) and a compressive region forms below it. This distribution of stress is reminiscent of that from an edge dislocation. We examine the possibility that the vacancy aggregate encompasses a dislocation by drawing a Burgers circuit around the void (Fig. 4(c)). This Burgers circuit shows

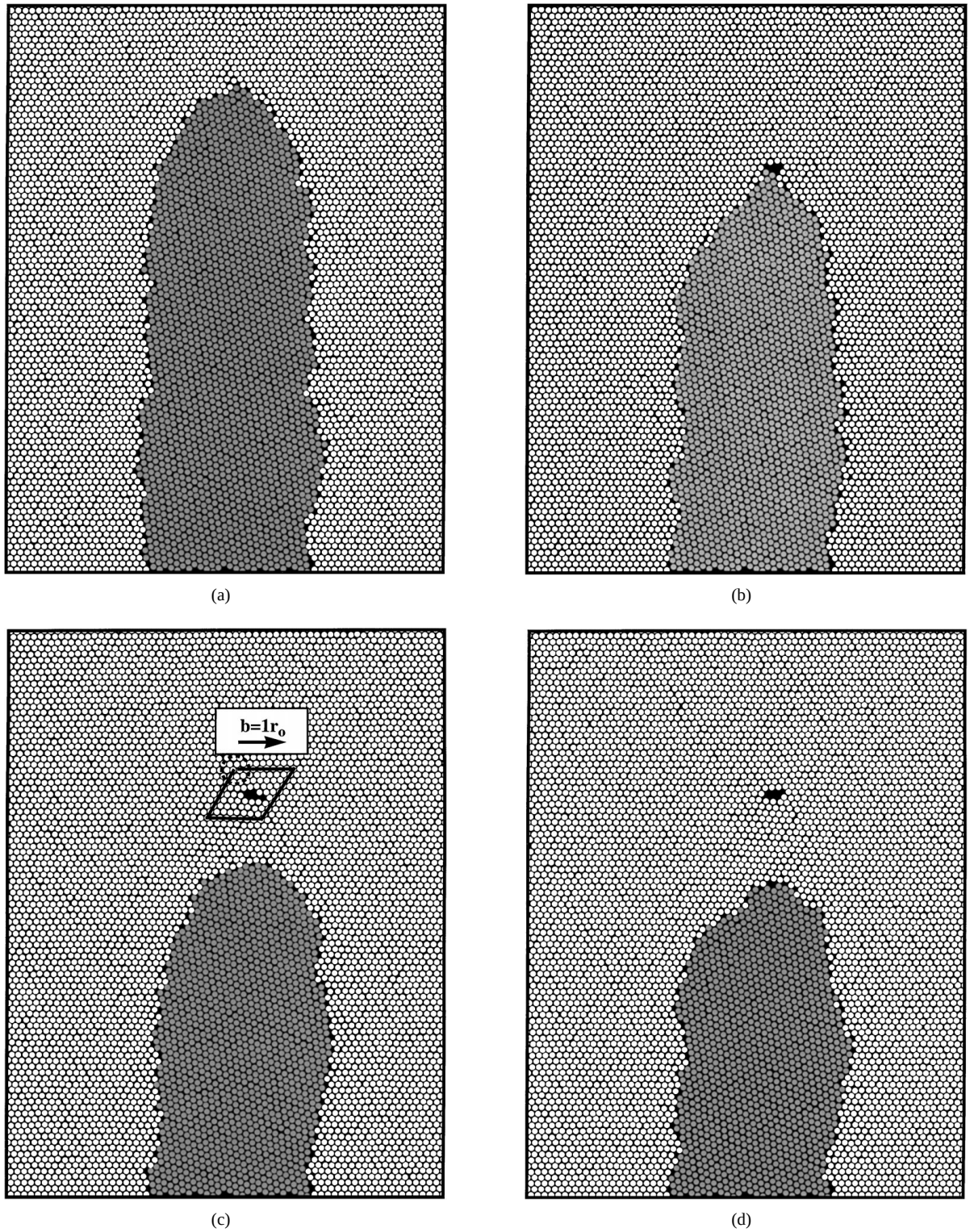

Figure 4. The temporal evolution of the atomic configuration of the retracting half-loop ($T = 0.175\varepsilon/k$ and $w = 21r_0$ and $\Sigma = 7\,(38.22^\circ)$), for which the half-loop area-time plot was shown in Fig. 3. Figures (a)–(j) correspond to $t = 50$, 200, 350, 440, 510, 615, 760, 800 and 860τ, respectively. Figure 4(c) shows a Burgers loop drawn around a void.

(*Continued on next page*.)

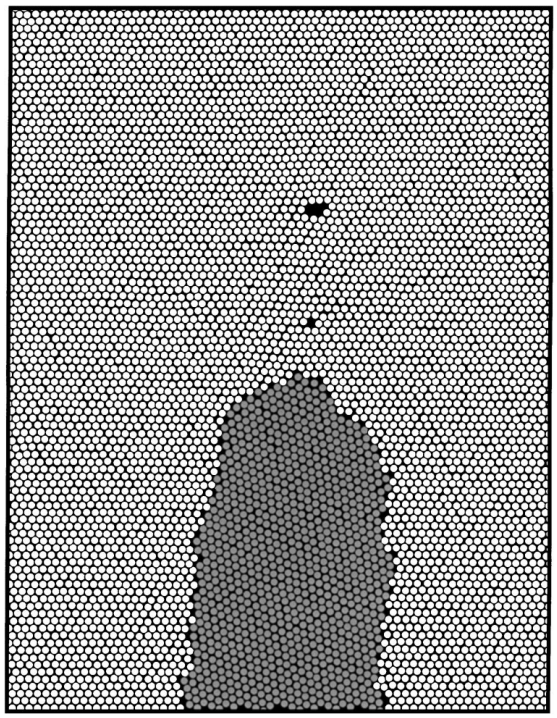

(e)

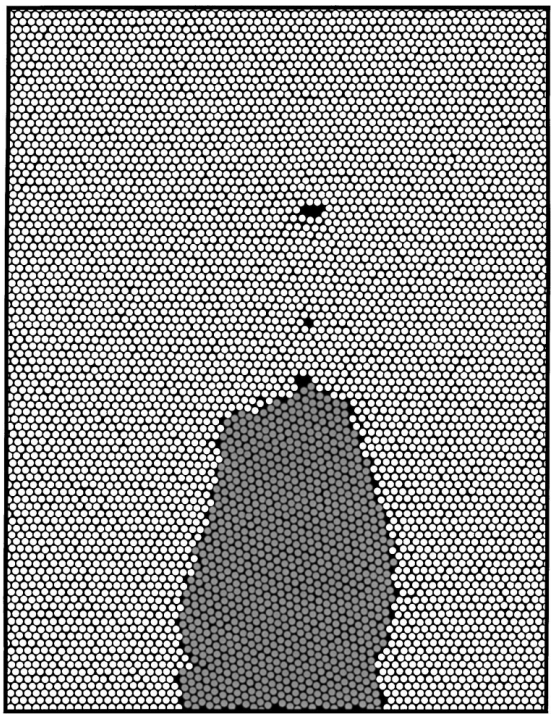

(f)

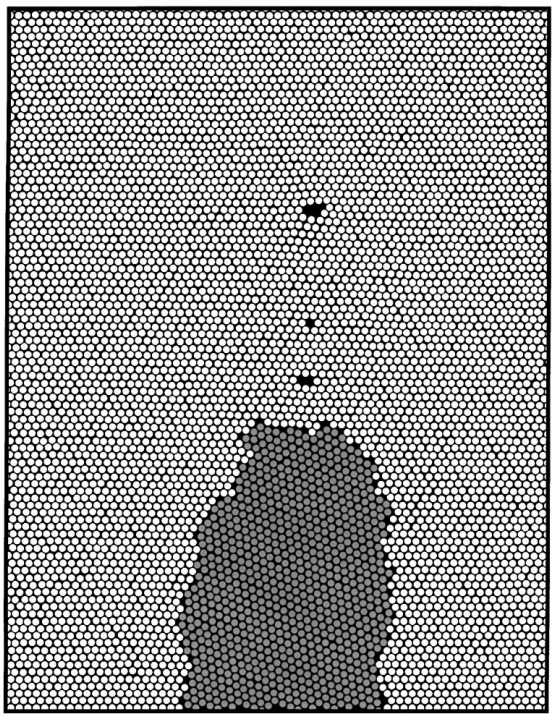

(g)

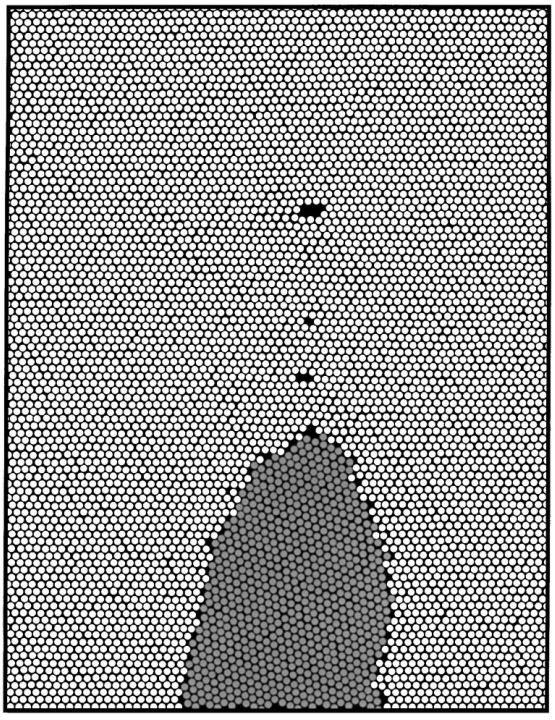

(h)

Figure 4.

(*Continued on next page.*)

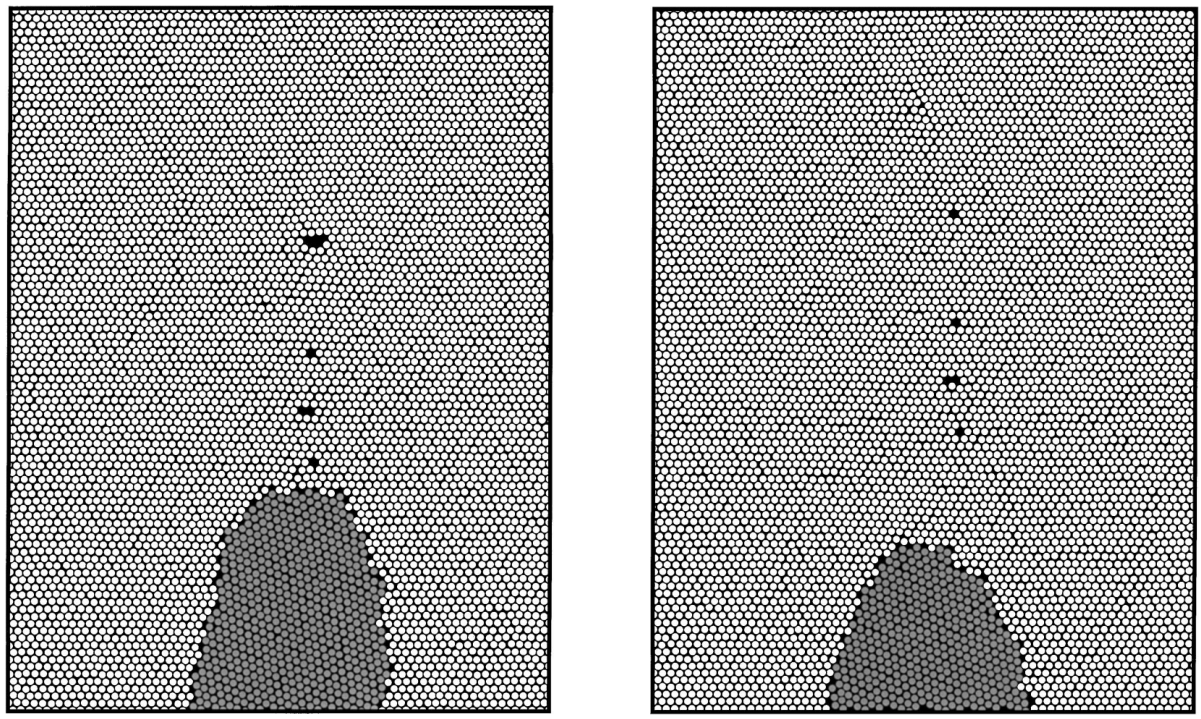

(i) (j)

Figure 4. (*Continued*).

that the vacancy aggregate contains an edge dislocation with Burgers vector $\vec{b} = r_0(1, 0)$. Examination of several atomic images following the grain boundary pull-off from the vacancy aggregates shows that the dislocation forms at the interface and then propagates up to and is captured by the void. The dislocation is presumably attracted into the void by elastic interactions with its free surfaces and remains there because of the same elastic effect and because the core energy of a dislocation inside a void is nearly zero. The ejected vacancy aggregate and the associated dislocation remain immobile after the grain boundary has pulled off. At late times, however, the vacancy aggregate begins to shrink and after the half-loop has shrunk to its minimum size, the void has completely disappeared (Fig. 4(j)). At this point, the dislocation becomes mobile and glides to the free surface of the simulation cell.

Following pull-off from the void, the half-loop migrates a finite distance, then slows again to a near plateau ($t \approx 450\tau$). Examination of the atomic configuration in Fig. 4(d) shows that a very small void (much smaller than in Figs. 4(a)–(c)) forms at the apex of the half-loop. This very small void is the apparent cause of the second plateau in Fig. 3 and a deviation from the steady-state-state half-loop shape. The grain boundary is able to pull away from the vacancy at $t \approx 475\tau$ and then quickly re-establishes a near steady-state shape and a resumption in the linear A vs. t kinetics (Figs. 4(e) and 3). In this case, the detached void is actually a single vacancy and contains no dislocation. This vacancy does not move significantly during the remainder of the simulations and sits at a finite distance below the first four vacancy void. This chain of events (void formation, slowing of half-loop shrinking, distortion of the boundary, void pull-off, re-establishment of steady state) repeats two more times during the simulation depicted in Figs. 3 and 4. A pair of vacancies are ejected at $t \approx 605\tau$ and a single vacancy at $t \approx 750\tau$ (see Figs. 3 and 4(f)–(i)). In both of these cases, the ejected vacancies remain immobile and they are not associated with dislocations. The present results provide clear evidence that much of the deviation from linearity in the A vs. t plot of Fig. 3 may be traced to vacancy formation on and pull-off from the migrating half-loop. This type of phenomena is both a common occurrence and is not accounted for in Eq. (1).

Like the half-loop boundary at high temperature ($T = 0.175\varepsilon/k$, $w = 21r_0$ and $\Sigma = 7\,(38.22^\circ)$)

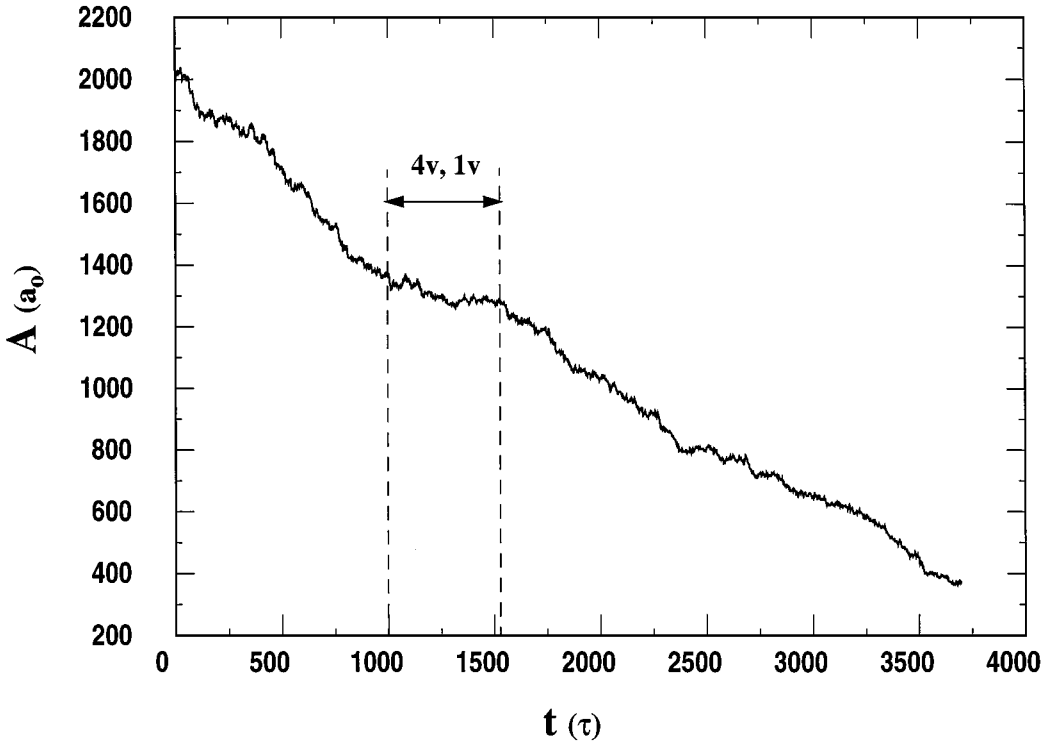

Figure 5. Variation of the area of the half-loop grain with time in a simulation performed at a low temperature ($T = 0.100\varepsilon/k$) for $w = 21r_0$ and $\Sigma = 7\,(38.22^\circ)$. The migration rate again plateaus for an extended time at $t = 1000\tau$. Two nano-voids, containing one and four vacancies, are ejected over the time period between the vertical dashed lines and indicated by the double headed arrows.

described above (Figs. 3 and 4), the same boundary at low temperature ($T = 0.100\varepsilon/k$) also shows vacancy formation. A plot of the half-loop area versus time is shown in Fig. 5 for this low temperature case. Following an initial transient, A decreases linearly with t, nearly plateaus at finite A, and then resumes its initial linear behavior. No other pronounced deviations from linearity are observed. The atomic configurations in this low temperature half-loop migration simulation are shown in Fig. 6. The steady-state migration of the half-loop in Fig. 6(a) is retarded by the simultaneous formation of two small voids at the top of the half-loop (Fig. 6(b)). The shape of the grain boundary half-loop changes dramatically when these voids form, becoming much sharper at the apex (Fig. 6(b)). This clearly occurs because the grain boundary is pinned at a (or two) point(s), while the remaining curved sections of boundary continue to migrate in an attempt to depin itself from the vacancies (Fig. 6(b)). At $t \approx 1400\tau$, the grain boundary pulls away, leaving behind two immobile voids. One void contains four vacancies, and the other is a single vacancy. The larger of these two voids is associated with a dislocation, as shown by the Burgers circuit drawn in Fig. 6(c). After pulling off the voids, the grain boundary reverts to its steady-state shape and linear shrinkage kinetics (Figs. 5 and 6(c)). No additional vacancies are ejected from the grain boundary at later times. Therefore, the major difference between the low and higher temperature cases is the number of vacancies omitted following the initial omission of a vacancy aggregate.

Additional simulations were performed for the $\Sigma = \infty\,(30^\circ)$ at elevated temperature ($T = 0.175\varepsilon/k$) and several half-loop widths. The resultant behavior and the atomic configurations (not shown) are very similar to those in Figs. 3 and 4 for the high symmetry ($\Sigma = 7\,(38.22^\circ)$) at high temperature; i.e., initial emission of a multi-vacancy aggregate followed by regular emission of single or di-vacancies. The only noticeable difference between the $\Sigma = 7$ and $\Sigma = \infty$ boundary results is that the emission of individual vacancies is delayed in the $\Sigma = 7$ relative to the $\Sigma = \infty$ case. Additional, simulations performed with a $\Sigma = 13$ boundary suggest that this distinction is likely associated with

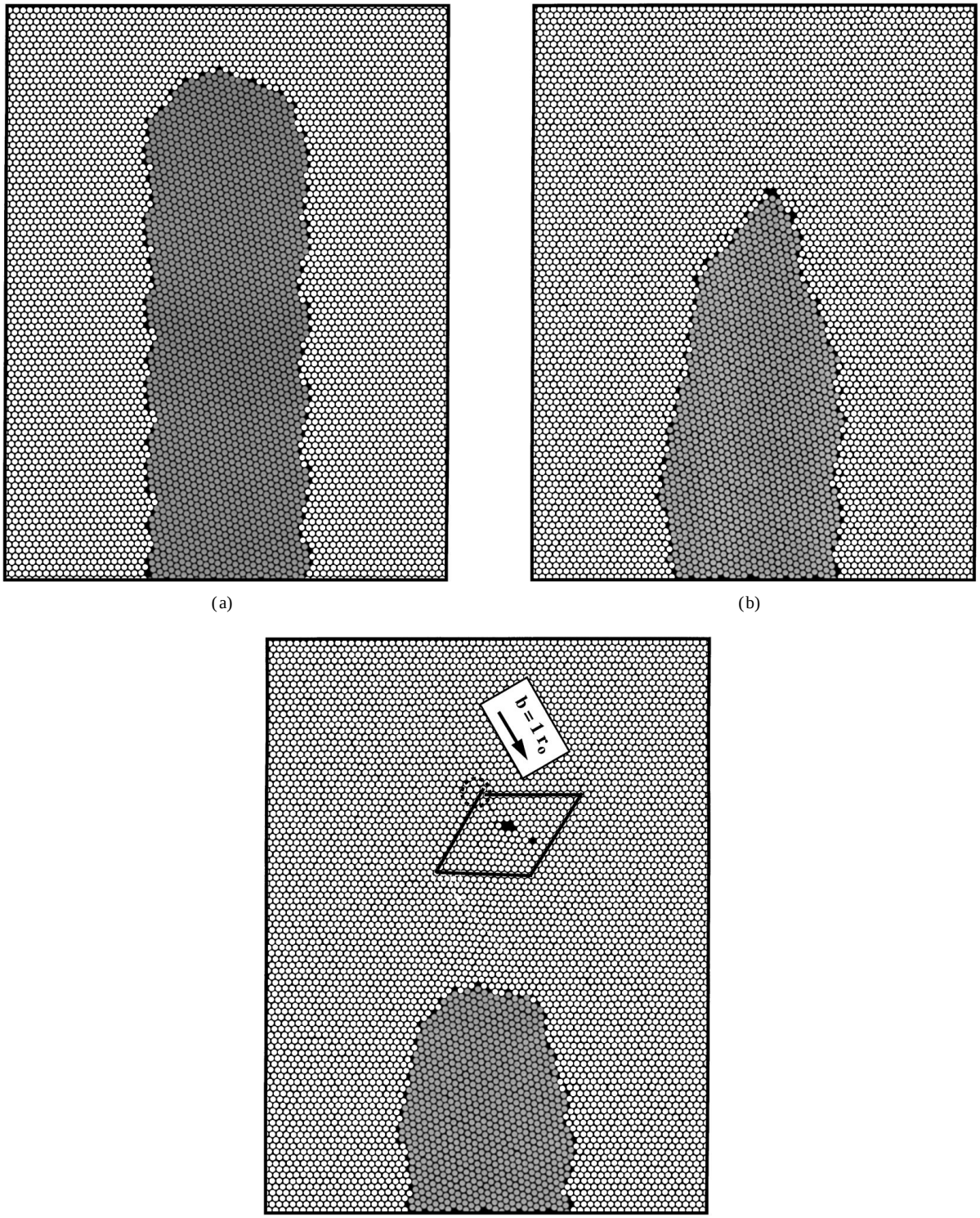

Figure 6. The temporal evolution of the atomic configurations of the retracting half-loop ($T = 0.100\varepsilon/k$ and $w = 21r_0$ and $\Sigma = 7\,(38.22^\circ)$), for which the half-loop area-time plot was shown in Fig. 5. Figures (a)–(c) correspond to $t =$ 500, 1200 and 3000τ, respectively.

Table 1. The number of vacancies emitted per void during the migration of the $\Sigma = 7$ (38.22°) half-loop grain boundary over a distance of $84r_0$ as a function of temperature.

Temperature (ε/k)	Vacancies emitted per void (a_0)		
	Simulation A	Simulation B	Simulation C
0.100	[4, 2]	[4, 1]	[4, 1, 1]
0.125	[3]	[3, 1]	[4, 1]
0.150	[5, 1]	[4, 1]	[4, 1, 1]
0.175	[4, 1, 2, 1]	[5, 1, 1, 1]	[4, 1, 1, 2]
0.200	[5, 1, 1]	[4, 2, 1, 1]	[5, 1, 1, 1]

Table 2. The number of vacancies emitted per void during the migration of the $\Sigma = \infty$ (30°) half-loop grain boundary over a distance of $84r_0$ as a function of temperature.

Temperature (ε/k)	Vacancies emitted per void (a_0)		
	Simulation A	Simulation B	Simulation C
0.100	[3]	[4]	[3]
0.125	[4]	[4, 1]	[5, 1]
0.150	[3,1, 1]	[2, 1, 1]	[3, 1]
0.175	[5, 1, 2, 1]	[4, 1, 2, 1]	[3, 1, 1, 1]
0.200	[3, 1, 2, 1]	[3, 1, 1, 2]	[3, 1, 1]

the differences between singular and general boundaries. Simulations performed at different half-loop widths indicate that the number of vacancies emitted under otherwise identical conditions is independent of half-loop width.

The number of voids ejected as the half-loop migrates over a distance of $84r_0$ and their size are reported in Tables 1 and 2 for three separate simulations over a range of temperature for singular $\Sigma = 7$ (38.22°) and general $\Sigma = \infty$ (30°) grain boundaries, respectively. It is evident from these tables that the first void to be emitted is an aggregate of several vacancies, the voids emitted subsequently consist of single or di-vacancies, that more vacancies are emitted per unit of migration as the temperature is raised, and that the general vacancy emission behavior is the same for the singular and general boundary.

4. Discussion

The results presented above clearly indicate that vacancy generation and emission is a common, if not intrinsic, component of curvature-driven grain boundary migration. In this section, we analyze why vacancies are generated and emitted, the number that are generated and emitted and why they are initially emitted in aggregates followed by single or di-vacancies.

As noted above, the first void to be emitted generally contains several vacancies and commonly contains an edge dislocation with the extra half plane of atoms directed, at least in part, in the $+Y$ direction (see Figs. 1 and 4). These interesting observations appear to be an artifact of the simulation, rather than intrinsic feature of grain boundary migration. The initial atomic configuration for these half-loop studies were constructed by inscribing the half-loop geometry onto two differently oriented crystals, disposing of the atoms from the outside on one and on the inside of the other and mating the two (being careful to remove atoms that were too close together). The grain boundary, constructed in this way has an excess volume above that of a relaxed boundary. When the molecular dynamics is turned on, the grain boundary structure relaxes and the excess volume must be accommodated elsewhere by the system. The edges of the simulation cell are left free such as to relax some of this volume by elastically displacing. The remaining excess volume is relieved as the boundary begins to migrate by forming a small (multi-vacancy) void at the top of the half-loop where the stresses are most hydrostatic (tension). This is the origin of the initial, multi-vacancy voids. Preliminary simulations which were performed with periodic boundaries in the X direction, tended to create larger voids. The presence of a dislocation in these voids is also a result of the initial conditions. The formation of an edge dislocation with a Burgers vector parallel to the X direction (and missing half plane of atoms below it) elastically compensates for the expansion of the lattice that occurred when inserting the grain within the half-loop. The shrinkage of the multi-vacancy voids at late times (see Figs. 4(h)–(j)) is associated with the presence of these dislocations and dislocation climb. This indicates that some of the excess volume is indeed relaxed elastically. Since these initial, multi-vacancy voids and their corresponding dislocations are an artifact of how the simulation was performed, they are omitted from the subsequent discussion.

The repeated generation of the vacancies and di-vacancies during boundary migration at elevated temperature is also associated with removing the excess volume from the system, however, in this case it is intrinsic. Since grain boundaries have an intrinsic excess volume, this excess volume must be accommodated

by the system when the boundary area decreases. In curvature-driven boundary migration, the total grain boundary area must decrease (this is one definition of curvature-driven boundary migration). This excess volume can be accommodated by creating elastic strains, modifying the structure of the grain boundaries or by generation of other defects that have excess volume, such as vacancies. Which effect dominates depends on the relative energetics of these competing accommodation methods. In simulations performed earlier, where periodic boundary conditions were enforced, the elastic energies associated with putting this excess volume directly into the lattice as strain was sufficiently large as to bias the system toward increased vacancy generation.

If all of the excess volume generated by the removal of grain boundary area was used to generate more vacancies, we can estimate the rate of vacancy generation. For the grain boundaries examined in this study, we measured the excess area/length (i.e., volume/area) to be $\alpha = 0.15 \pm 2r_0$ for $\Sigma = 7$ (38.22°) and $0.22 \pm 3r_0$ for $\Sigma = \infty$ (30°). If the half-loop migrates a distance ΔL, this implies a generation of excess area (volume) of $2\alpha\Delta L$, since two boundaries of length ΔL are destroyed. The area (volume) associated with a single vacancy is $3\sqrt{3}r_0^2/8$. Therefore, one vacancy should be generated for each ΔL of boundary migration, where ΔL is

$$\Delta L = \frac{3\sqrt{3}}{16\alpha} r_0^2. \tag{2}$$

For the $\Sigma = 7$ (38.22°) boundary this corresponds to $\Delta L = 2.2r_0$ and for the $\Sigma = \infty$ (30°) boundary $\Delta L = 1.5r_0$. While these distances are very short, it is important to recall that this rate of vacancy generation is independent of half-loop width. Therefore, although this rate of generation is large when the widths are as small as those used in the present simulation, this rate (number generated per width per unit migration) would be several thousand times smaller for a grain size of 10 μm. In our simulations, the grain boundaries traverse large distances before they release vacancies.

In Fig. 4 (high temperature, $\Sigma = 7$), between the emission of the initial, multi-vacancy void and the emission of the first individual vacancy (i.e., Figs. 4(b) and (d)), the grain boundary traverses a distance of $12r_0$. It then traverses a distance of $6r_0$ before it ejects the di-vacancy, and then a further $4r_0$ before it ejects the last vacancy. Clearly, the rate of vacancy emission increases as the half-loop shrinks but even at its fastest, the emission rate is roughly 80% smaller than that predicted from Eq. (2). The acceleration of vacancy emission is likely a result of changing elastic constraint. As the top of the half-loop gets closer and closer to the rigid bottom of the simulation cell, the free surfaces in the $\pm X$ directions are less able to elastically transfer the excess volume to the surface. The theoretical values predicted by Eq. (2) should only be valid in the limit where no elastic accommodation is possible.

The vacancy generation frequency and the tendency to form di-vacancies was found to increase with increasing temperature (see Tables 1 and 2). Presumably, both of these observation can be attributed to the increased ease with which grain boundaries can form vacancies at higher temperatures. This is not surprising since the transport of excess volume from one region of a grain boundary to another is likely a thermally activated process. The relatively infrequent vacancy generation at low temperatures suggests that the excess volume generated by grain boundary migration can be accommodated, to some degree, by the boundary structure itself or elastically since neither are strongly thermally activated. The low temperature situation is one in which slow kinetics prevents the attainment of the low energy state. Di-vacancies occur in greater at elevated temperatures because more vacancies are generated in close proximity to each other under those conditions.

Grain boundaries pull themselves off voids by sharpening in the region of the pinning point. This sharpening occurs because the boundary continues to migrate down except at the pinning point. The sharper the boundary gets at the pinning point, the greater is the driving force to pull off the pinning point in a method akin to how grain boundary and dislocations pull off of pinning particles. In these latter cases, a critical angle is often used as a pull-off condition in analytical theories. At higher temperatures, thermal fluctuations can make pull-off even easier. Comparison of Figs. 4(a) and 6(a) show that the $\Sigma = 7$ grain boundary has a higher tendency to facet at lower temperatures than at higher temperatures, presumably due to the anisotropy in grain boundary mobility (as discussed by the authors in [16]). The presence of facets at low temperature could make it more difficult for the tip of the boundary to sharpen near the pinning point, thereby making it more difficult for the boundary to pull off of the generated vacancy. This in turn will further slow the boundary and lead to less vacancy generation at low temperature. The sharpening of the grain boundary at the pinning point also has analogies in the grain boundary-impurity studies

of Lücke and Detert [22] and Aristov et al. [18]. In the latter, where the shape of the grain boundary studied was the same as in the present study, impurity drag was found to sharpen the tip of the U-shaped half-loop sharper. In an experimental study of triple junctions by Galina et al. [23], triple junction drag led to sharper angles at the triple junctions. Triple junction and vacancy drag both play the same role in sharpening the loop.

The present simulations were all performed using Lennard-Jones potentials. These potentials are known to have several deficiencies for describing metals, the most important for the present simulations being that they are too stiff in compression. The deficiencies in this interatomic potential could lead to excess grain boundary volumes which are too large compared with experiment (or simulation using other, such as EAM, potentials) or relaxations of vacancy cores not in accord with experiment, such that the quantitative observations reported herein are not reliable. However, the main qualitative features of the present simulation results (i.e., vacancy generation as a result of curvature-driven boundary migration) should be robust to specific choice of interatomic potentials in these close packed systems.

5. Conclusion

The present atomistic simulations clearly demonstrate that curvature-driven motion of grain boundaries (i.e., boundary migration to decrease the boundary area) results in the generation of excess volume that must be accommodated by some mechanism. If the grains are constrained such that they cannot elastically transfer the excess volume to the free surface, the grain boundaries will generate and emit vacancies. Such vacancy production was observed here. The rate at which vacancies are generated is determined by many factors, including the excess volume (per unit area) of the grain boundaries, the temperature and the degree of constraint in the surrounding grains. While vacancies are readily generated by grain boundaries at elevated temperature, this generation is suppressed at low temperature. If the grain boundaries easily emit the generated vacancies, the vacancies have little effect on the boundary motion. On the other hand, at low temperature, vacancies that are generated tend to pin the grain boundaries until sufficient boundary curvature at the pinning point is generated (by boundary migration) to enable the boundary to pull away. If the grain boundaries are incapable of generating vacancies (sufficient free volume transport is necessary to accumulate the volume necessary to produce a vacancy), then the build up of elastic strain energy would counteract the capillary driving force and prevent additional boundary migration.

Acknowledgments

M.U. and D.J.S. gratefully acknowledge the financial support of the Division of Materials Science of the Office of Basic Energy Sciences of the United States Department of Energy Grant #FG02-88ER45367, under whose auspices this research was performed. L.S.S. and G.G. express their gratitude to the Deutsche Forschungsgemeinschaft and to the Russian Foundation for Fundamental Research under contract N 96-02-17483 for financial support for their collaboration.

References

1. R.W. Balluffi, Phys. Stat. Sol. (B) **31**, 443 (1969).
2. A.P. Sutton and R.W. Balluffi, *Interfaces in Crystalline Materials* (Clarendon Press, Oxford, 1995), p. 522.
3. J.P. Hirth and J. Lothe, *Theory of Dislocations*, 2nd edition (Wiley, New York, 1982), p. 746.
4. K.L. Merkle and D.J. Smith, Phys. Rev. Lett. **59**, 2887 (1987); Ultramicroscopy **22**, 57 (1987).
5. G.J. Woods, W.M. Stobbs, and D.J. Smith, Phil. Mag. A **50**, 375 (1984).
6. M. Cheikh, A. Hairie, F. Hairie, G. Nouet, and E. Paumier, Colloque de Phys. **51**, C1-103 (1990).
7. R.C. Pond and V. Vitek, Proc. R. Soc. London B **357**, 453 (1977).
8. S.P. Chen, D.J. Srolovitz, and A.F. Voter, J. Mater. Res. **4**, 62 (1989).
9. D. Wolf and S.R. Phillpot, Mat. Sci. Eng. A **107**, 3 (1989).
10. A. Sutton, Phil. Mag. A **60**, 147 (1989).
11. D.J. Srolovitz, G.S. Grest, and M.P. Anderson, Acta Metall. **33**, 2233 (1985).
12. G.J. Wang and V. Vitek, Acta. Metall. **32**, 951 (1986).
13. K. Lücke and G. Gottstein, Acta Metall. **29**, 779 (1981).
14. Y. Estrin and K. Lücke, Acta Metall. **29**, 791 (1981).
15. H. Gleiter, Acta Metall. **27**, 187 (1979).
16. M. Upmanyu, R.W. Smith, and D.J. Srolovitz, Interface Science **6**, 41 (1998).
17. V.E. Fradkov and L.S. Shvindlerman, Phys. Chem. Mech. Surfaces **1**, 180 (1982).
18. V.Y. Aristov, V.E. Fradkov, and L.S. Shvindlerman, Sov. Phys. Solid State **22**, 1055 (1980).
19. V.Y. Aristov, Y.M. Fridman, and L.S. Shvindlerman, Phys. Met. Metall. **35**, 859 (1973).
20. F.C. Frank, *Metal Surfaces* (ASM, Metals Park, Ohio, 1962), p. 1.
21. D.J. Srolovitz, N. Sridhar, J.P. Hirth, and J.W. Cahn, Scripta Materialia, (1998), in press.
22. K. Lücke and K. Detert, Acta Metall. **5**, 628 (1957).
23. A.V. Galina, V.Ye. Fradkov, and L.S. Shvindlerman, Phys. Met. Metall. **63**, 165 (1987).